Planetary and Stellar Parameter Fitting WASP-12b using ELC

Department of Astronomy, San Diego State University

ABSTRACT

We observed the exoplanet WASP-12b on one night in April 2015 at Mount Laguna Observatory, capturing the latter half of its transit. The lack of ingress hampered our attempt to extract the stellar and planetary parameters, thus we supplemented our data with previous work by Maciejewskiet al. (2011), Hebb et al. (2009), and light curves provided by amateur astronomical observers at the Czech Astronomical Society. Error bars for these data were generated based on the standard deviations outside of transit; a similar process was used to estimate MLO uncertainties, with modifications made to reflect the changing airmass throughout the night. System parameters were fitted with a genetic algorithm built into Orosz and Hauschildt's (2000) Eclipsing Light Curves modeling code, and these were found to agree reasonably well with previous work, with the exception of those tied to limb darkening, which was not well modeled in this attempt. The overall reduced x^2 was 1.14.

1. Mount Laguna Observatory

1.1. Hardware and Observations

I-band photometry of WASP-12b was obtained at the 1.0 m telescope at Mount Laguna Observatory ("MLO"). The camera on this instrument is a 2048 × 2048 CCD 2005 with a plate scale of 0.41 arcseconds/pixel, though we cropped the view to 512 × 1536 to decrease readout time and reduce clutter in the field of view. We took flat-field images inside the dome; due some delay during this process and to the lateness of sunsetwe were not able to capture ingress of the WASP-12b transit. The sky was cloudless and moonless, though winds reached up to 26 mph at times. FWHM varied between 4.25 – 4.5 pixels until after egress, when airmass climbed past 2.5 and FWHM rose to approximately 6 pixels.

1.2. Processing of MLO Data

All data calibration was done with AstroImageJ[1], an open-source image processing program based on the NIH's ImageJ software. AstroImageJ ("AIJ") provides a detailed

[1] Available for free download at http://www.astro.louisville.edu/software/astroimagej/. AstroImageJ is distributed under the GNU General Public License.

graphical user interface for working with FITS images, and thus serves as an acceptable alternative to IRAF for a project at this level.

AIJ built a master bias image from the 11 bias images from MLO, and then subtracted this master bias from the science images. Similarly, the 11 flat images were built into a master flat and used to normalize the science images. On the resulting calibrated images, apertures were placed around WASP-12 and four nearby comparison stars, and AIJ recorded counts (ADU) and flux for these objects and the surrounding sky on each image.

We converted the resulting flux data to magnitudes and normalized it to 0.0. Eastman's online Coordinated Universal Time (UTC) to Barycentric Julian Date in Barycentric Dynamical Time (BJD_TDB) calculator (Eastman et al. 2010) was used to convert the local times to a format more useful for comparison with other light curves. After these steps, comparison with the simultaneous sky light curve (Fig. 1.2) indicated that further trimming of the data was necessary, as during the initial recording the near-twilight sky had been bright and quickly changing. 65 points were discarded, i.e., all those taken prior to BJD 2457138.64454358.

1.3. Error Bars on the MLO Data

AIJ generated estimated error bars for the data it calibrated, but during the fitting process it became clear that these uncertainties were overestimated and not representative of the data. Though its reported errors were not identical for each point, they did not reflect the clear change in data quality that resulted from the higher airmass at the end of the evening. To alleviate this issue, we discarded those error bars, and assigned new errors based on the standard deviations of the data taken through specific airmass ranges.

Considering only the out-of-transit times (when the airmass began to change significantly), we divided the data into sections based on the airmasses at their associated times: those with airmass less than 2.5 (between BJD 2457131.720167274 and x1.741004339), those between airmass 2.5 and 3.0 (between BJD 2457131.741221319 and x1.755330008), and those with airmass greater than 3.0 (between BJD 7131.755546988 and 1.761190464). The standard deviation was calculated separately for each section, and each of the out-of-transit data points were then assigned error bars equal to the standard deviation of their section; since the "airmass > 3.0" section had the highest standard deviation, those points had the largest error bars, while the "airmass < 2.5" section had the smallest. This process was taken under the assumption that the out-of-transit light curve should be flat, hence it is appropriate for a system whose star is not particularly active.

Finally, since standard deviation would not be an appropriate measure of data scatter for the curves in the signal during transit, those data were assigned error bars equal to the smallest of the out-of-transit standard deviations. Note that by choosing the smallest possible error bars, the x^2 is less likely to be underestimated than if larger error bars were assigned. The resulting light curve is plotted in Fig. 1.3.

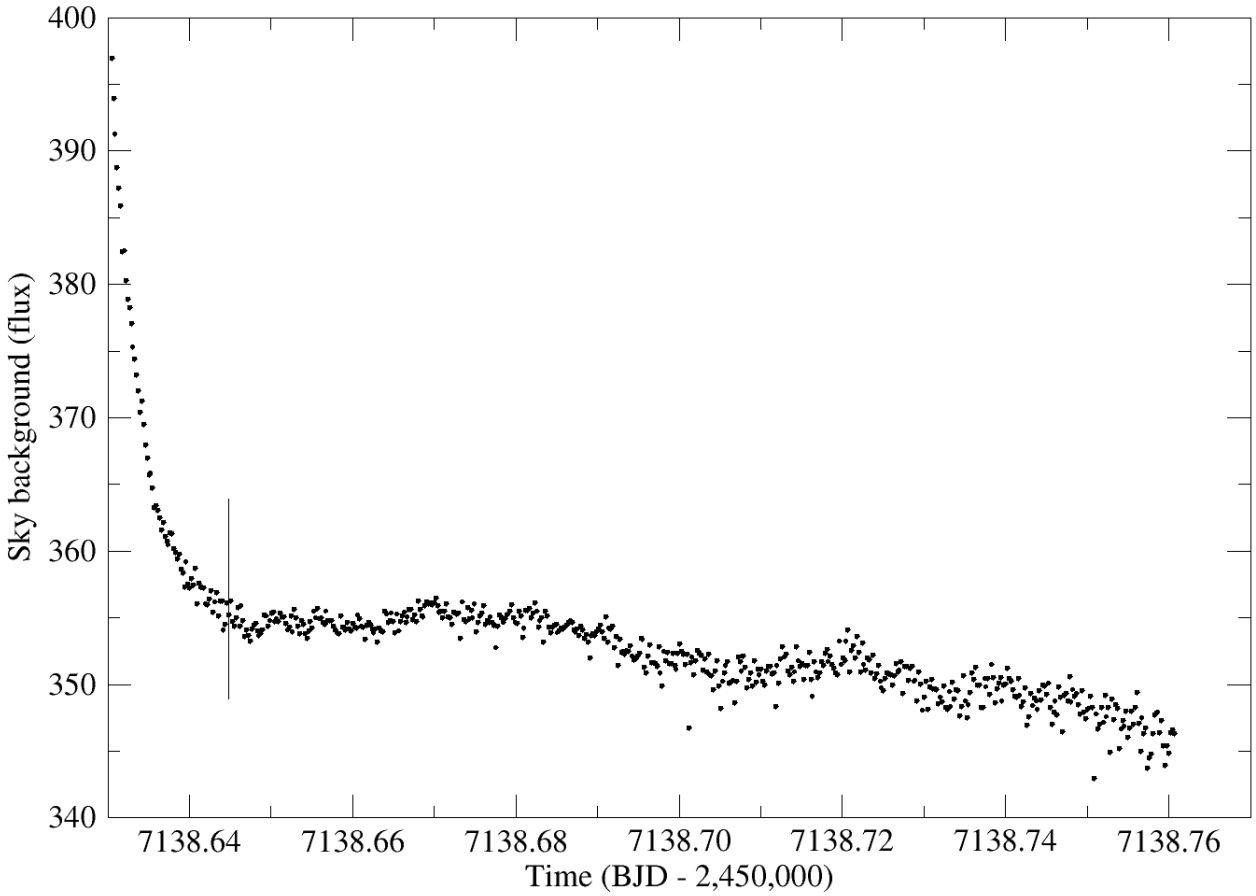

Fig. 1.— Sky brightness at Mount Laguna Observatory during the entire observing of WASP-12b. Data taken prior to BJD 2457138.64454358, indicated by the vertical line, were discarded due to the high sky brightness.

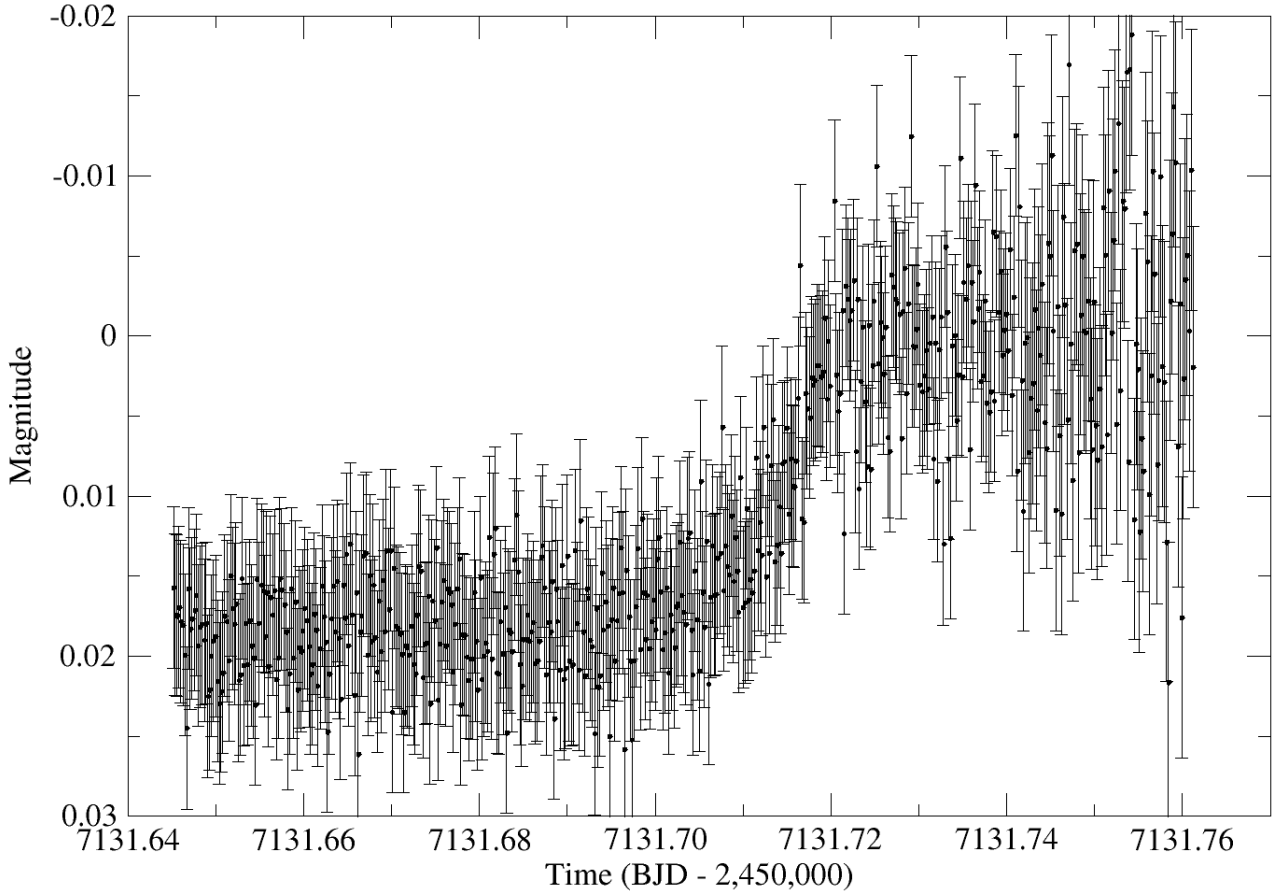

Fig. 2.— Light curve for WASP-12b transit, as observed from Mount Laguna Observatory on 18 April 2015. Error bars were calculated assigned to the standard deviations of the post-transit points; see Section 1.3 for details.

2. Additional Transit and Radial Velocity Data

To supplement the partial transit obtained from MLO, we obtained additional I-band and R-band data from the Exoplanet Transit Database of the Czech Astronomical Society [2] a repository of data observed and maintained by "amateur" astronomers. Though this database's 153 WASP-12b light curves vary greatly in quality, each is given a rating from 1 to 5 ("best" to "worst"), allowing for easy selection of useful data.We selected two R-band curves of quality "2", as well as one I-band curve of quality "3." There was only one quality "2" light curve available in the I-band, but it had some features that proved problematic during parameter fitting, hence the supposedly lower-quality curve was selected instead.

Since most of these light curves did not come with uncertainty estimates, or had associated uncertainties of questionable origins, we assigned new error bars to them based on the same standard deviation method outlined in Section 1.3.For each, the standard deviation for the entire out-of-transit curve was calculated and assigned as error bars for the entire transit. We omitted the sectioning procedure, since the out-of-transit scatter was mostly constant.

Maciejewski et al. (2011) provided a third R-band light curve, and Hebb et al. (2009) gave radial velocities for WASP-12. We did not adjust the error bars of these data.

3. Parameter Fitting

3.1. Fitting Process

We fit thirteen parameters of WASP-12b with the Eclipsing Light Curve ("ELC") code of Orosz & Hauschildt (2000) using its a genetic algorithm optimization procedure (geneticELC). The genetic algorithm was allowed 100 "members" in each generation, with 1500 generations generated. Reasonable starting points were selected based on previous values obtained by Maciejewski et al. (2011) and Hebb et al. (2009). Due to the short period of the system, the time of initial transit (T_0) and period (P) needed to be tightly constrained to produce reasonable results, but other parameters were allowed to roam over wider ranges. These ranges, and the resulting best-fit values, are given in Table 1.

The eccentricity was fixed at 0.0, based on the nearly-circular possible values for this parameter discussed by Maciejewski et al. (2011). We also assumed quadratic limb darkening, with initial values as suggested by Claret & Bloeman (2011) for a star with $\log(g_*) = 4.00$, $T_{\rm eff} = 6250$ K, $\log[M/H] = 0.3$, and $v_{\rm turb} = 2.0$ km/s. The first of these values was chosen to match that given by Maciejewski, and the rest attempt to match the Hebb results; though these "matches" are far from ideal (especially for microturbulent velocity, $v_{\rm turb}$, which Hebb gives as 0.85 km/s), Claret & Bloeman do not provide any closer parameter options. The

[2] Accessible via http://var2.astro.cz/ETD/

fitted limb-darkening parameters appear in Table 2.

3.2. Results

geneticELC generated separate models for each data set, but fit the same set of parameters to the entire collection. The resulting model transits are plotted in Figures 3.2 - 3.2. Each model light curve provides a reasonable fit to its data set, though all but the amateur I-band data have some "bumps" in the residuals near egress that indicate that limb darkening is not being modeled perfectly. The limb-darkening parameters reported in Table 2 also indicate trouble with limb darkening, as the I-band parameters are borderline unphysical. Fig. 3.2 and Fig. 3.2 show the x^2 values that resulted from geneticELC's "guesses" of these parameters during optimization.In contrast, the R-band x and y limb-darkening are well-converged (Fig. 3.2 and Fig. 3.2).

The physical implications behind this limb-darkening trouble are unclear. A rough calculation from the stellar radius and mass puts the density of WASP-12 at 0.43 g/cm^3, or 0.31 $\rho_\odot$. This result is significantly lower than those discovered by Maciejewski et al. (2011) (4.14 ± 0.09 $\rho_\odot$) and Hebb et al. (2009) (4.17 ± 0.03 $\rho_\odot$), indicating a major flaw in this modeling attempt. In the same vein, the planet-to-star temperature ratio is similarly off from previous results (see Table 1).A more accurate model of stellar temperature may provide a base for more accurate limb darkening, since T_* is partially responsible for the opacity in the stellar atmosphere, but such an improvement would require a wider variety of measurements (e.g., metallicity) than we have available from the MLO run. Stellar atmosphere models could probably also improve the modeling by making up for any deficiencies in the quadratic limb darkening model.

With the exception of stellar density, almost all other parameters fitted (e.g., see Fig. 3.2 and Fig. 3.2) were within or near the uncertainty ranges of Hebb et al. (2009) and Maciejewski et al. (2011). Stellar mass (see Fig. 3.2) and the star-to-planet radii ratio (Fig. 3.2) were somewhat small,but these parameters are lightly linked to those discussed above, so small deviations there are consistent with these results. Finally, the radial velocity model is plotted against the Hebb et al. (2009) RV data in Fig. 3.2. Again, the results agree reasonably well with the data, with only some consistent deviations near phase 0.8.

Overall, the reduced x^2 of the entire data and model set was 1.14, reasonably close to the ideal value of 1.0 given the limb darkening difficulties.

REFERENCES

Claret, A., & Bloeman, S. 2011, A&A, 529, A75

Eastman, J., Siverd, R., Gaudi, B. S. 2010, PASP, 122, 894

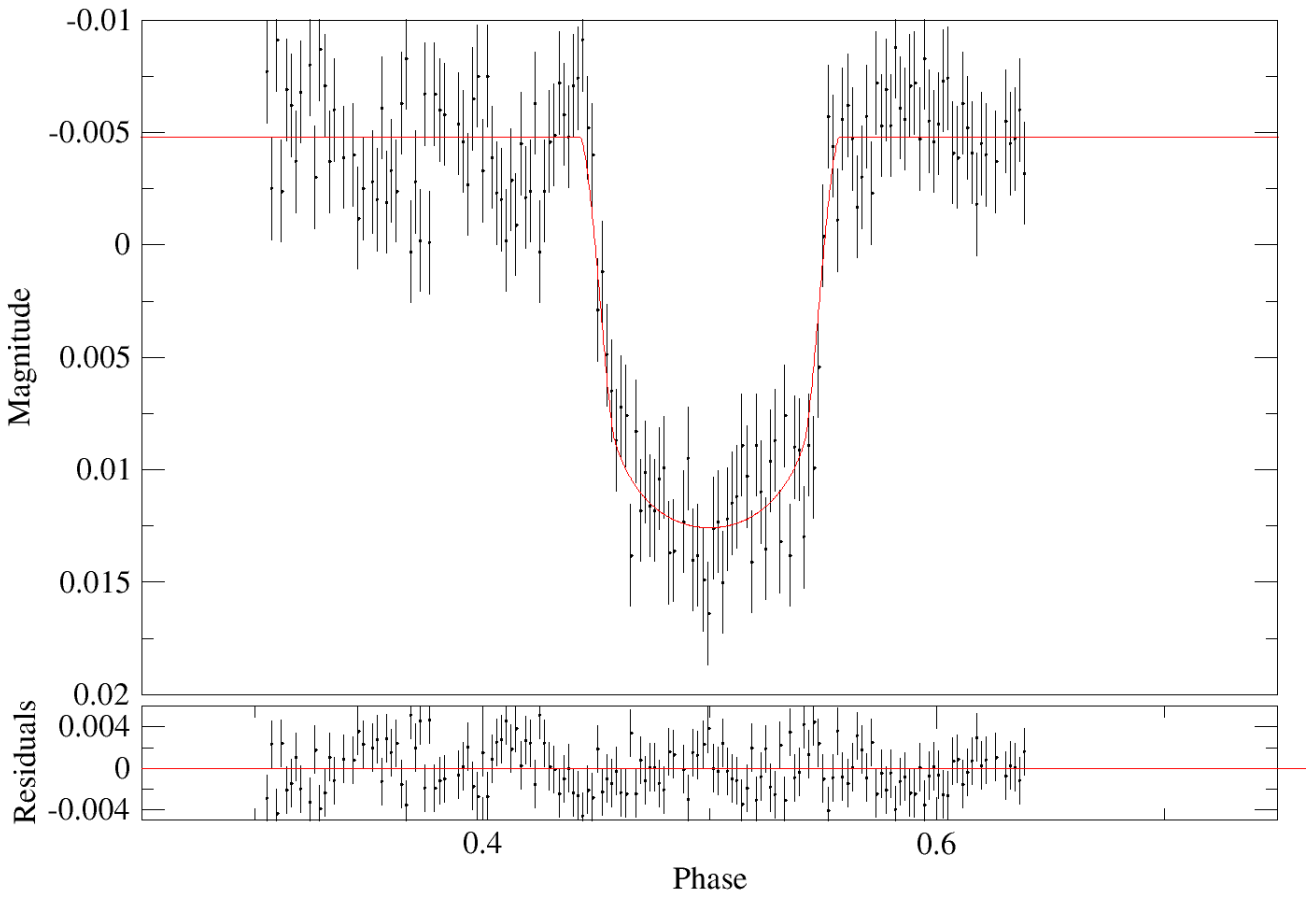

Fig. 3.— ELC model for the first R-band amateur light curve, plotted with the corresponding data and residuals. Error bars for this data set were generated as described in Section 1.3.

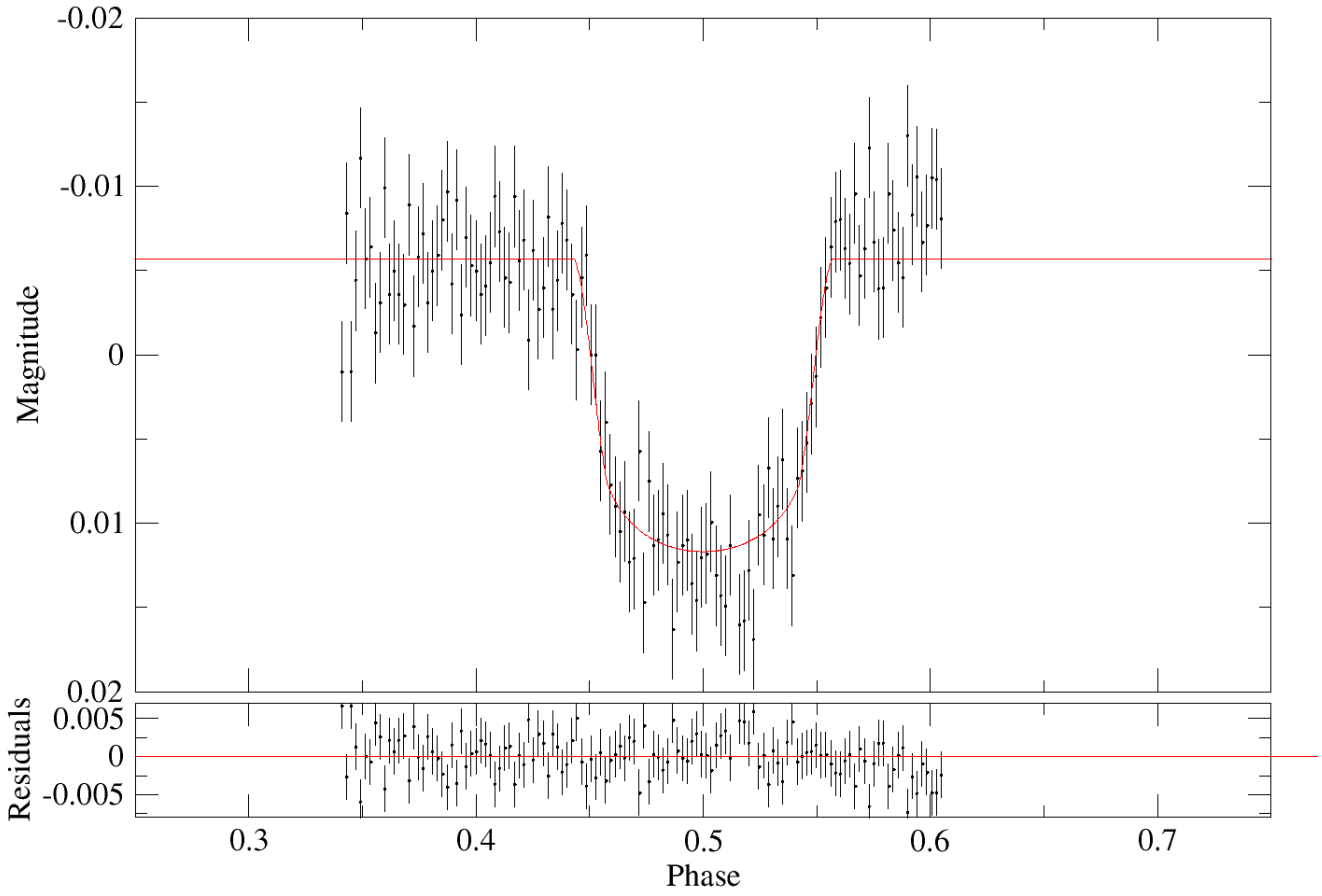

Fig. 4.— ELC model for the second R-band amateur light curve, plotted with the corresponding data and residuals. Error bars for this data set were generated as described in Section 1.3.

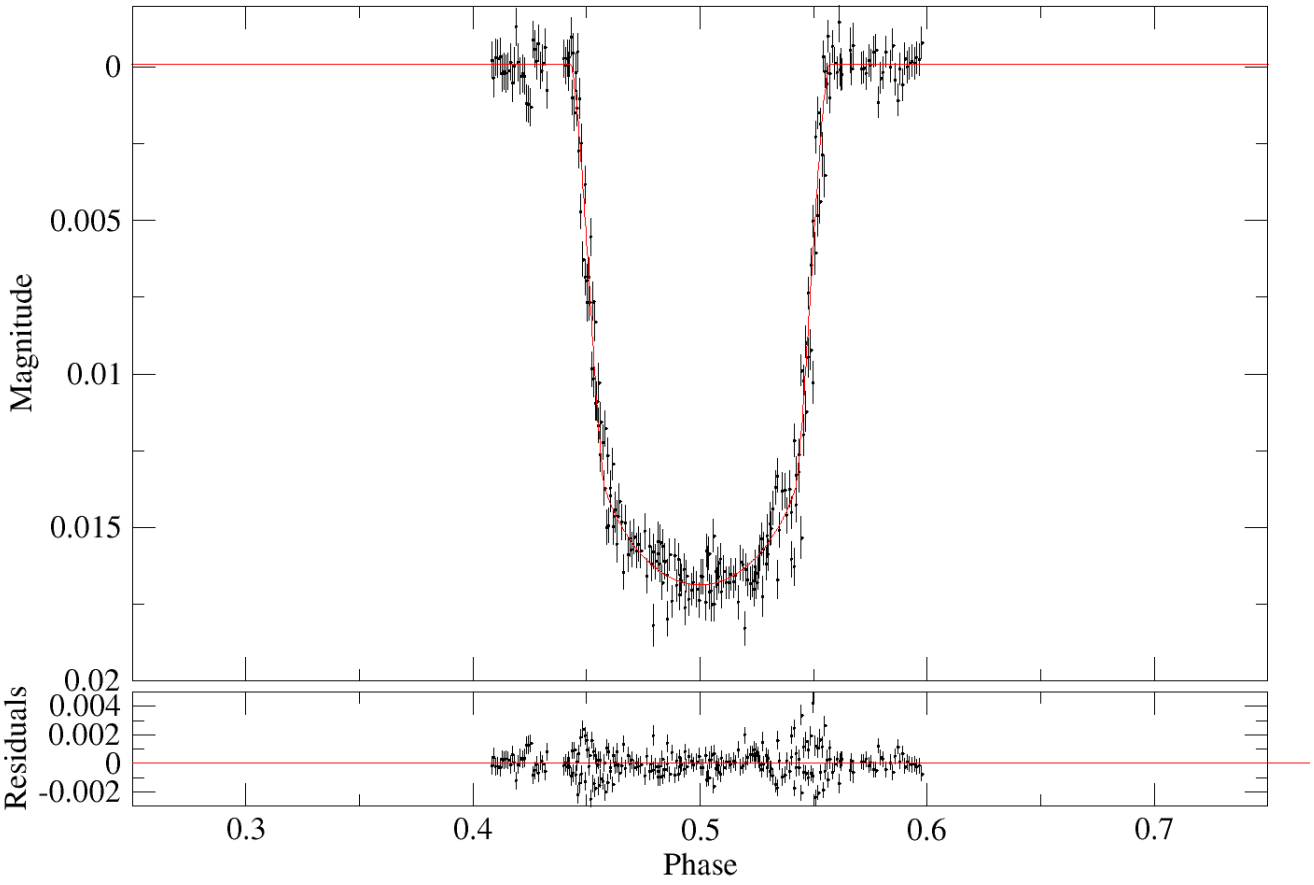

Fig. 5.— ELC model for the R-band Maciejewski et al. (2011) data, plotted with the corresponding data and residuals.

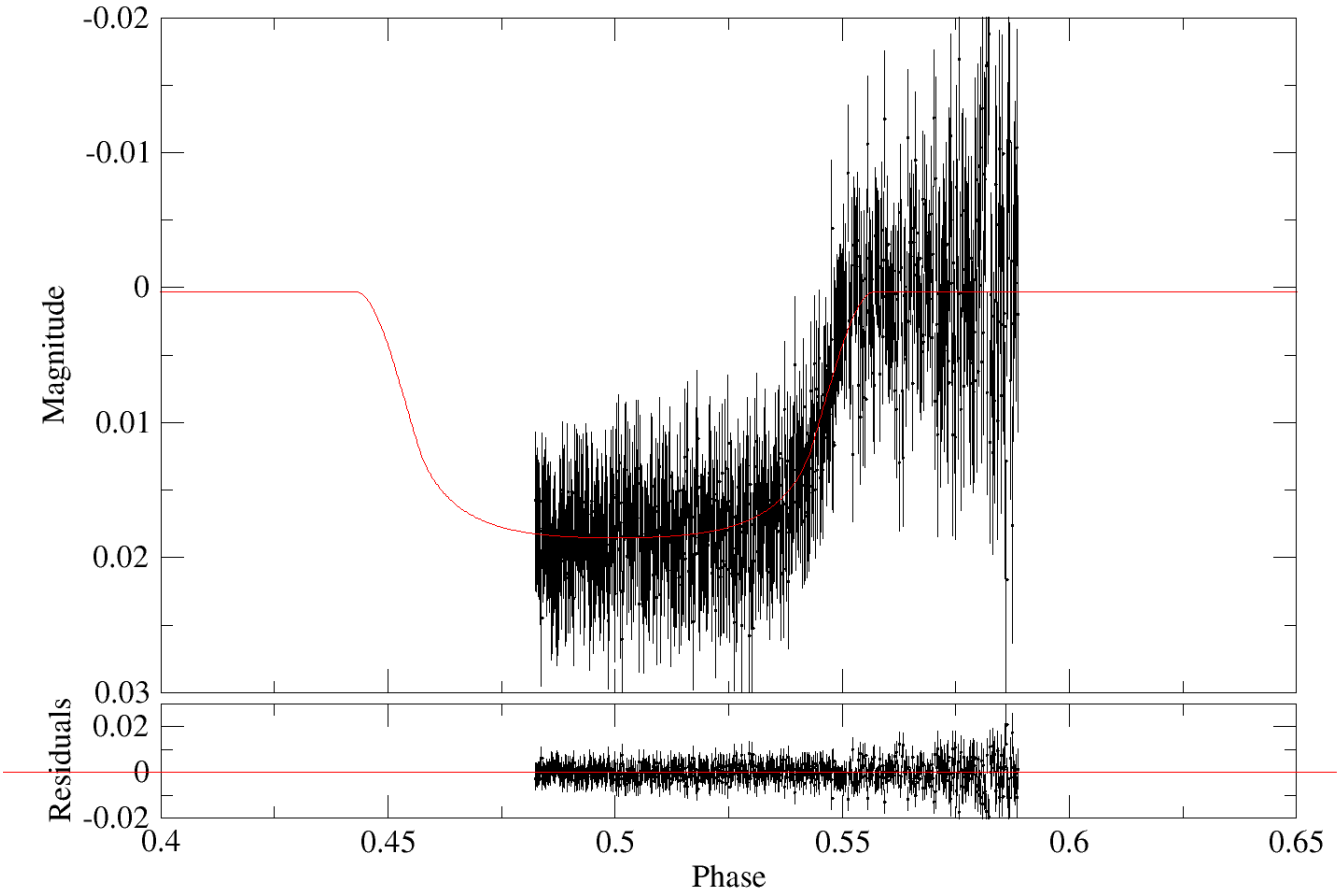

Fig. 6.— ELC model for the MLO light curve, plotted with the corresponding data and residuals. Error bars were generated as described in Section 1.3.

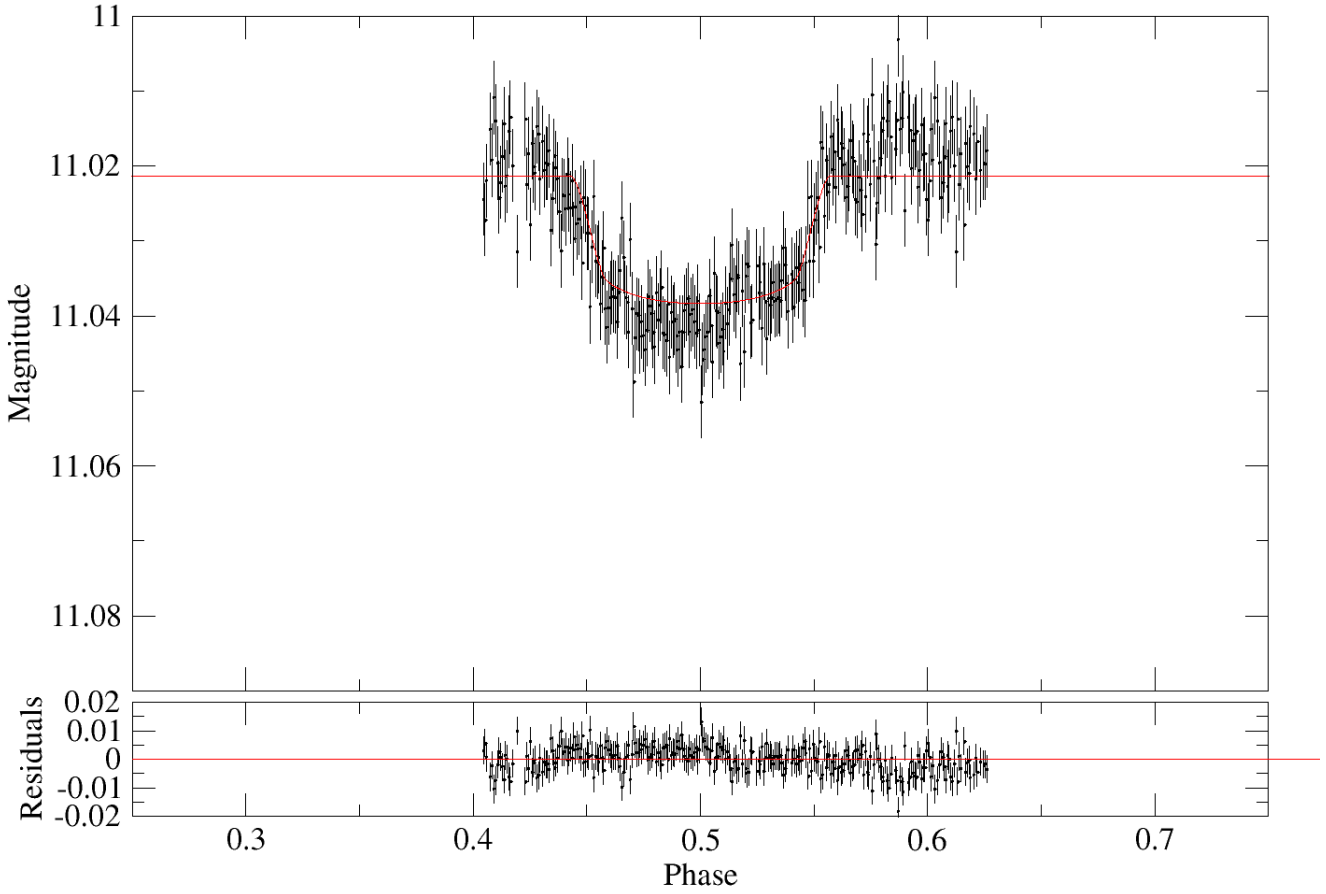

Fig. 7.— ELC model for the amateur I-band light curve, plotted with the corresponding data and residuals. Error bars for this set were generated as described in Section 1.3.

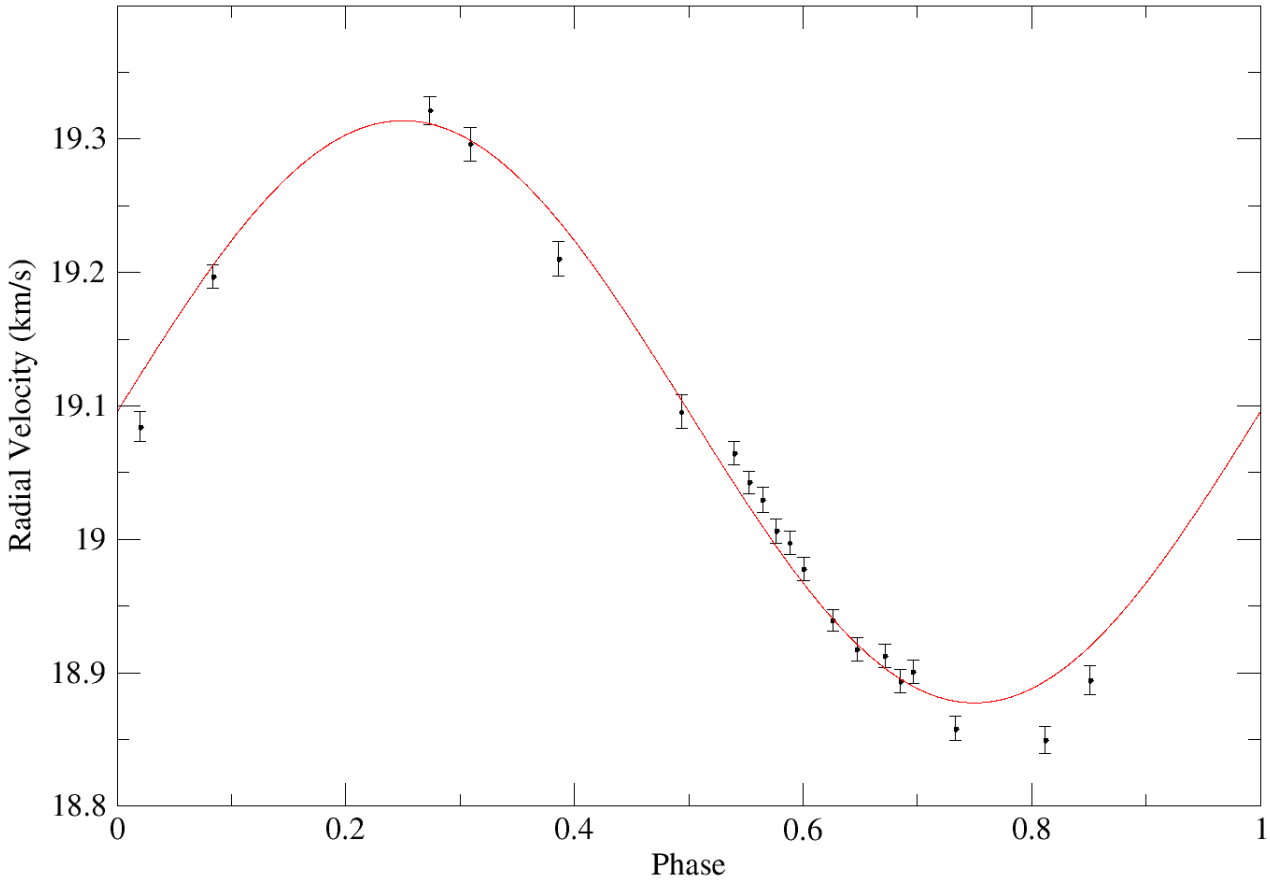

Fig. 8.— ELC model for the radial velocity curve, plotted with the Hebb et al. (2009) data and resulting residuals.

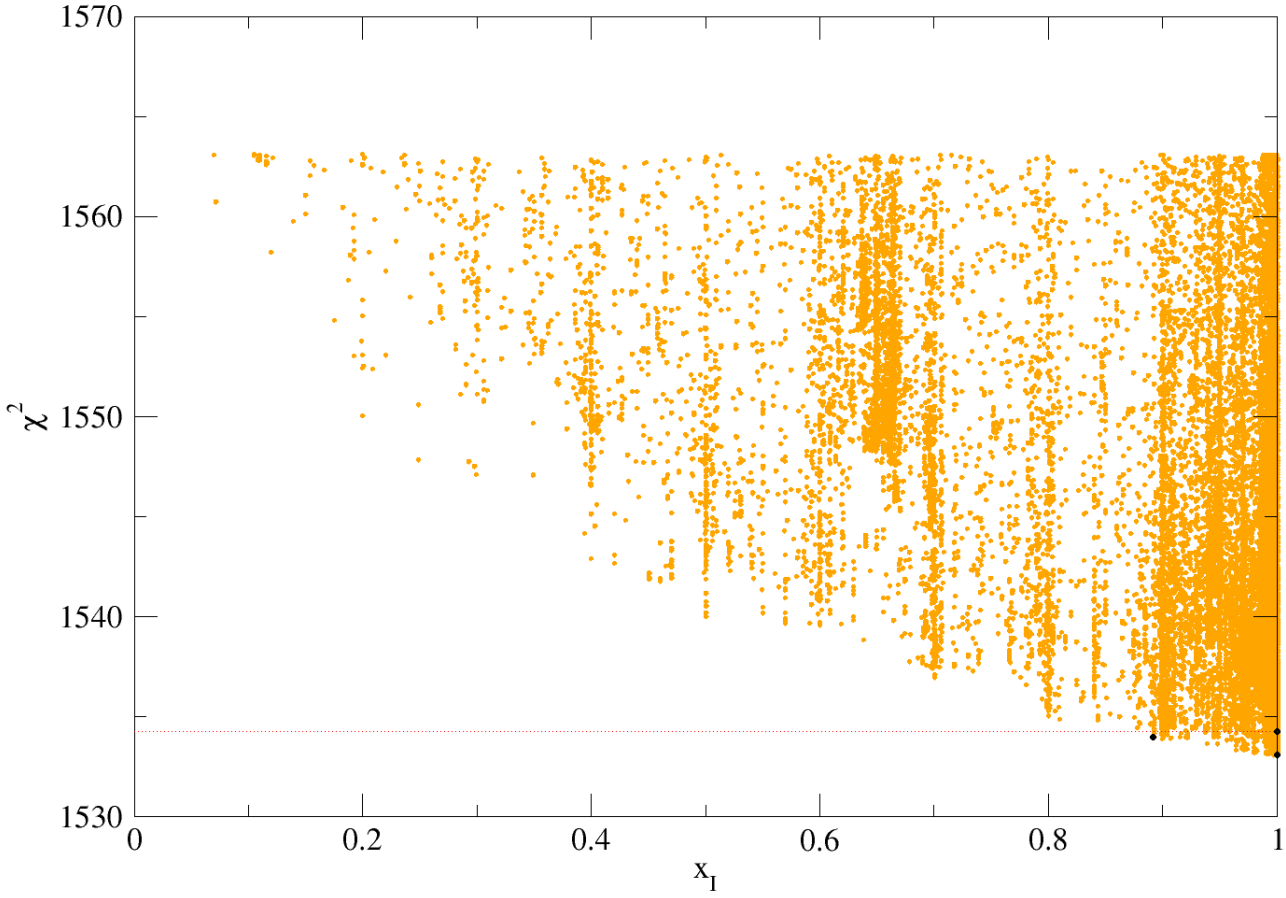

Fig. 9.— x^2 values resulting from geneticELC's guesses for x_I during its 1500-generation run. The optimizer clearly pushed x_I toward its upper limit, set at 1.0 to maintain physicality.

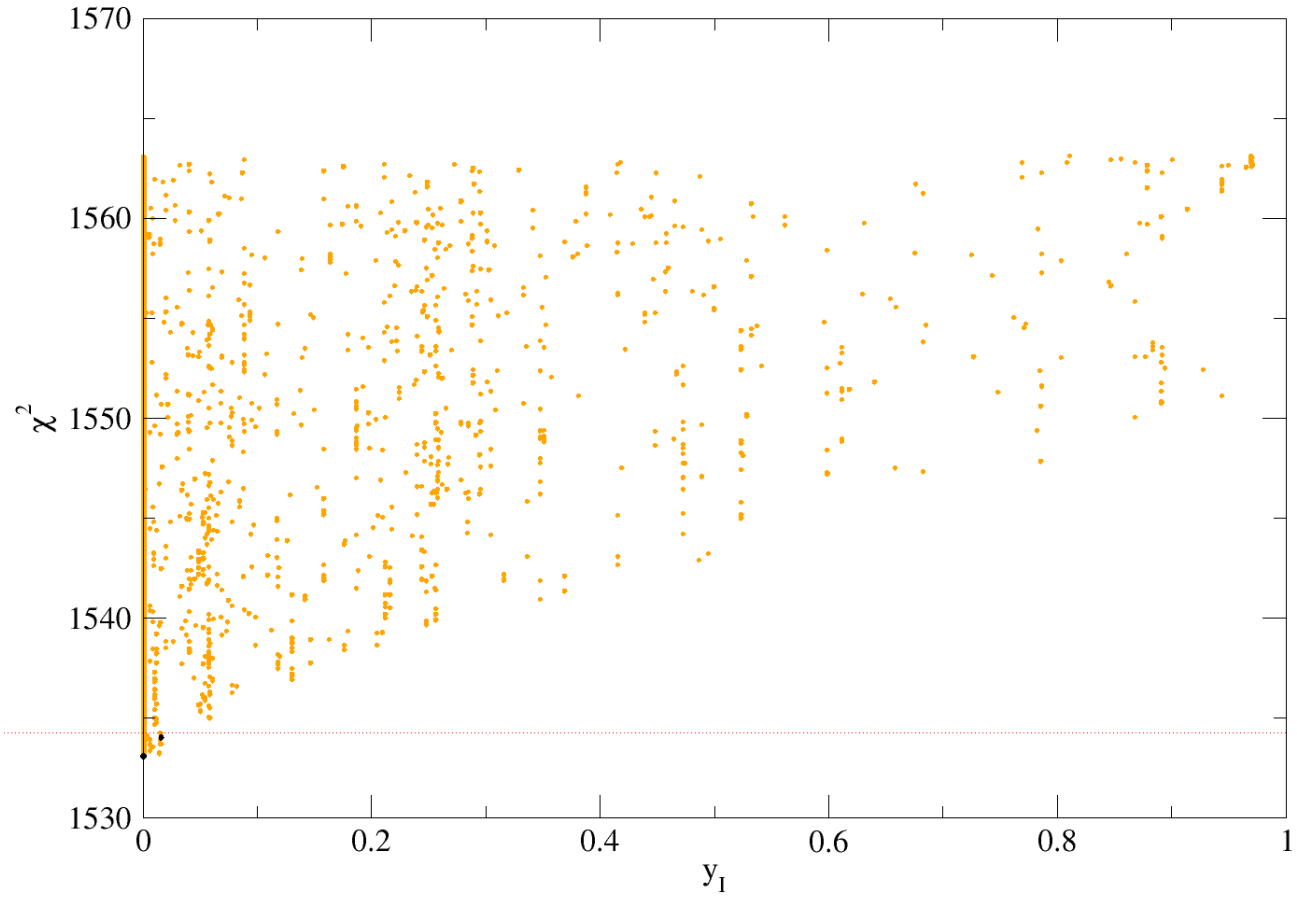

Fig. 10.— x^2 values resulting from geneticELC's guesses for y_I during its 1500-generation run. The optimizer clearly pushed y_I toward 0.0, though that parameter was permitted to vary to as low as −1.0.

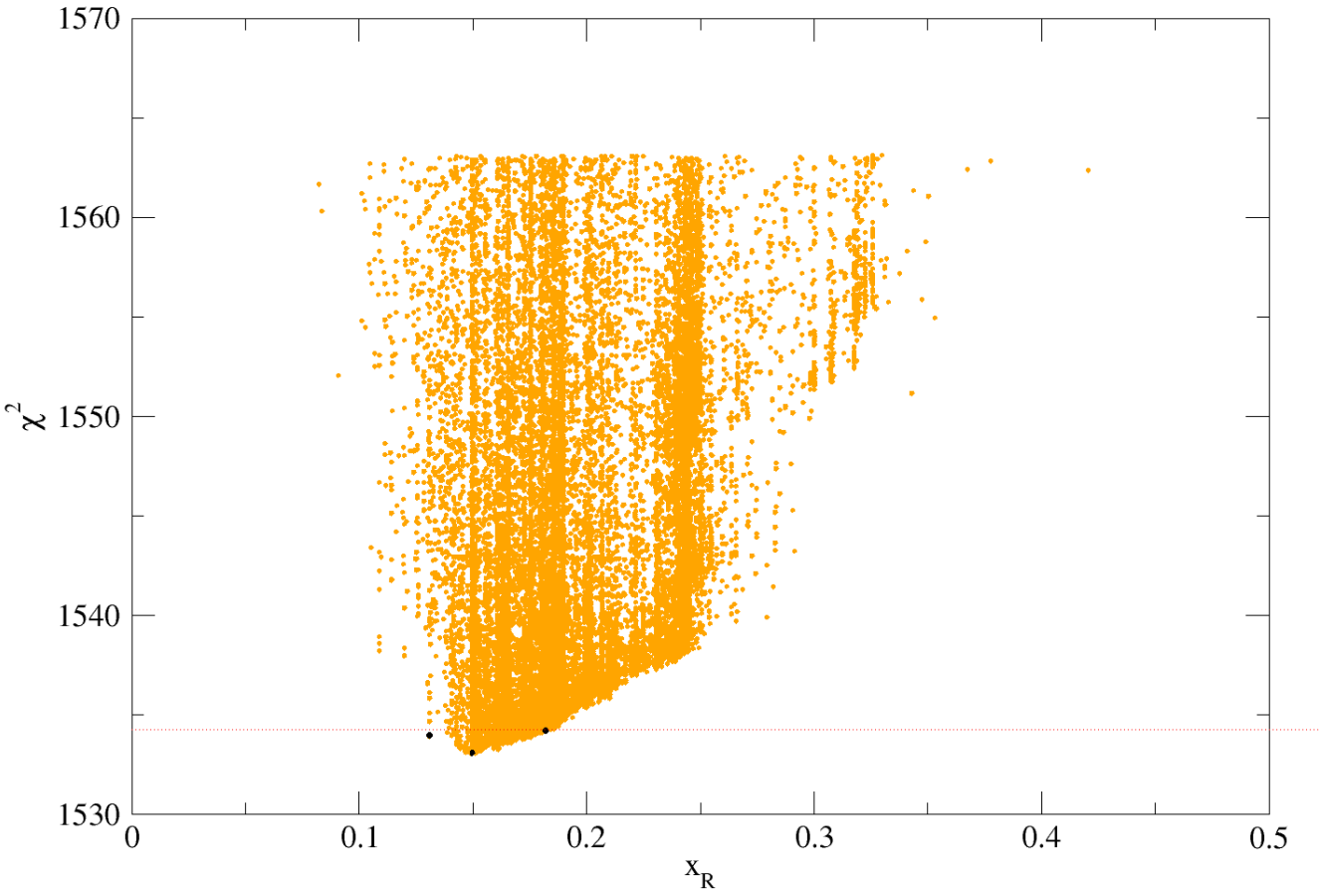

Fig. 11.— x^2 values resulting from geneticELC's guesses for x_R during its 1500-generation run. The values are well-converged.

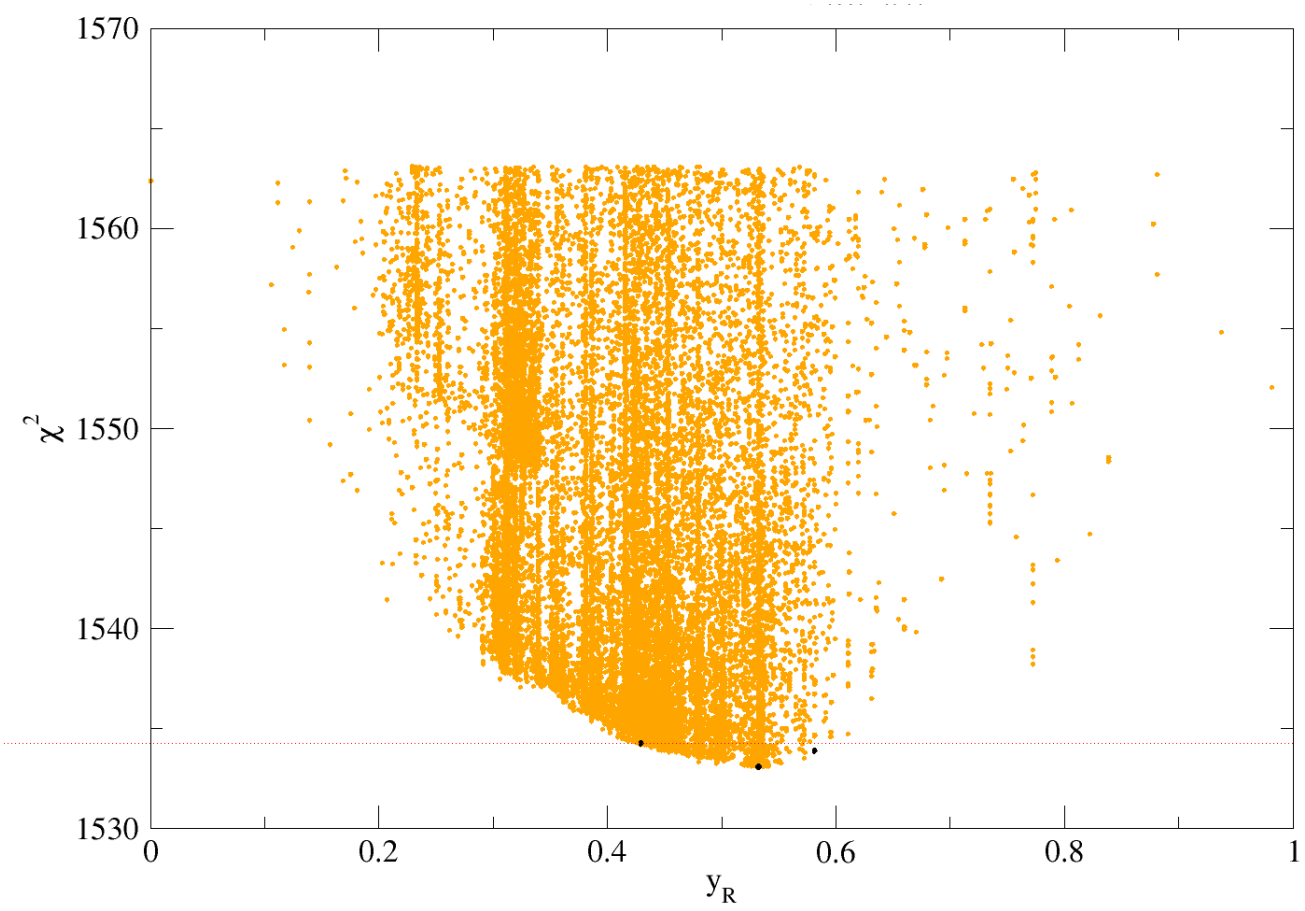

Fig. 12.— x^2 values resulting from geneticELC's guesses for y_R during its 1500-generation run. The values are well-converged.

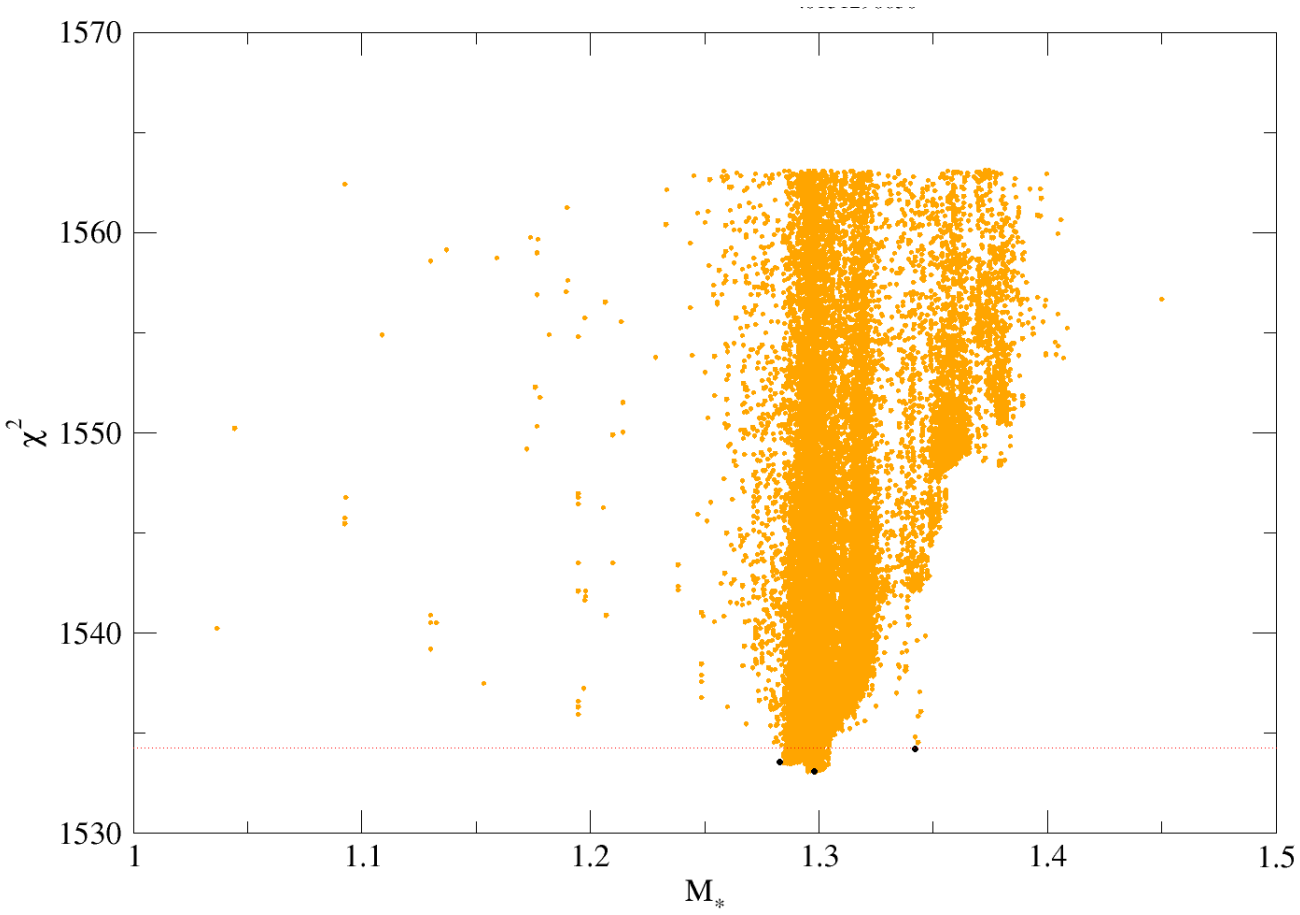

Fig. 13.— x^2 values resulting from geneticELC's guesses for M_star during its 1500-generation run. The values are not quite well-converged; additional generations or tighter constraints could potentially provide clearer results.

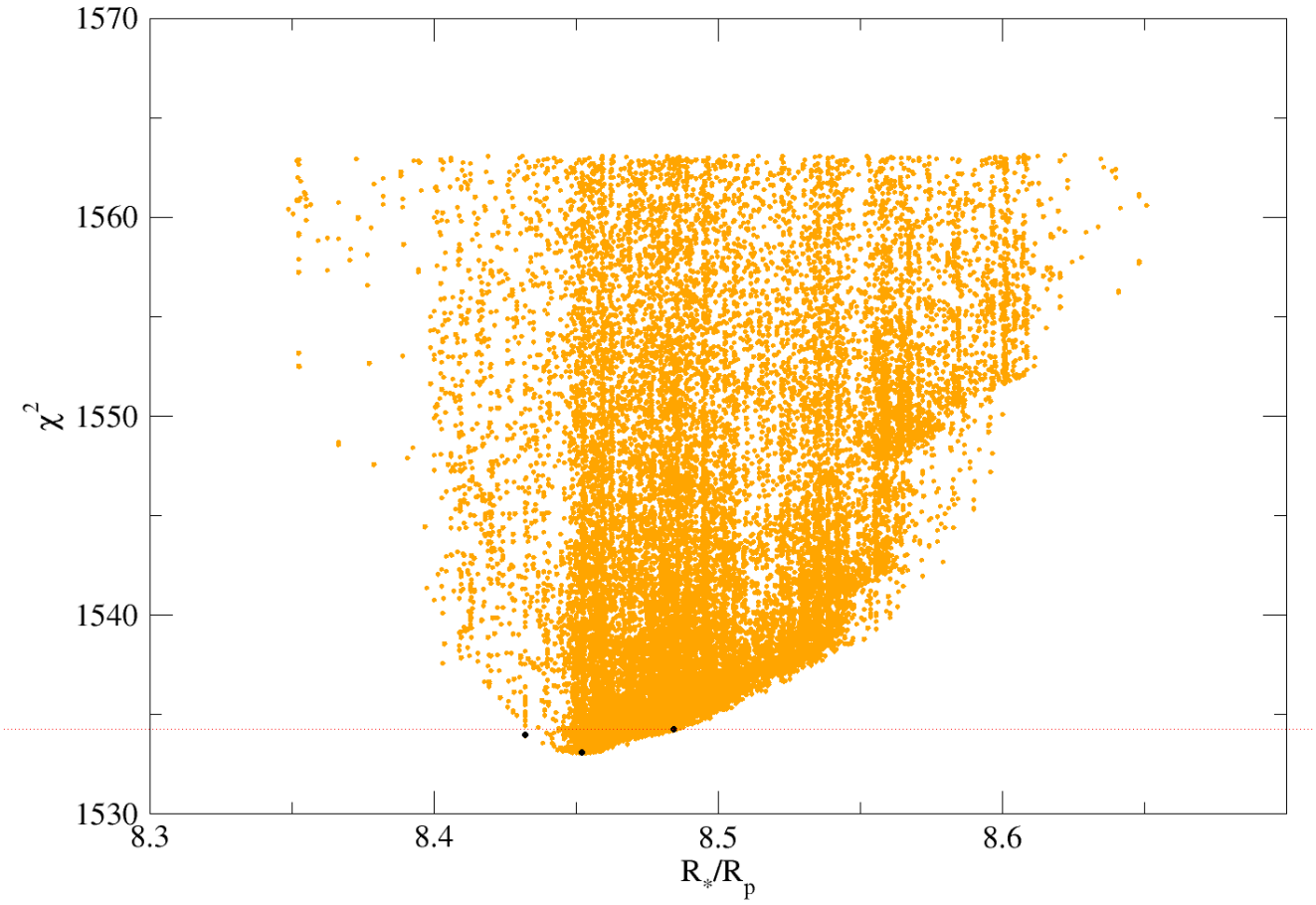

Fig. 14.— x^2 values resulting from geneticELC's guesses for R_*/R_p during its 1500-generation run. The values are mostly well-converged.

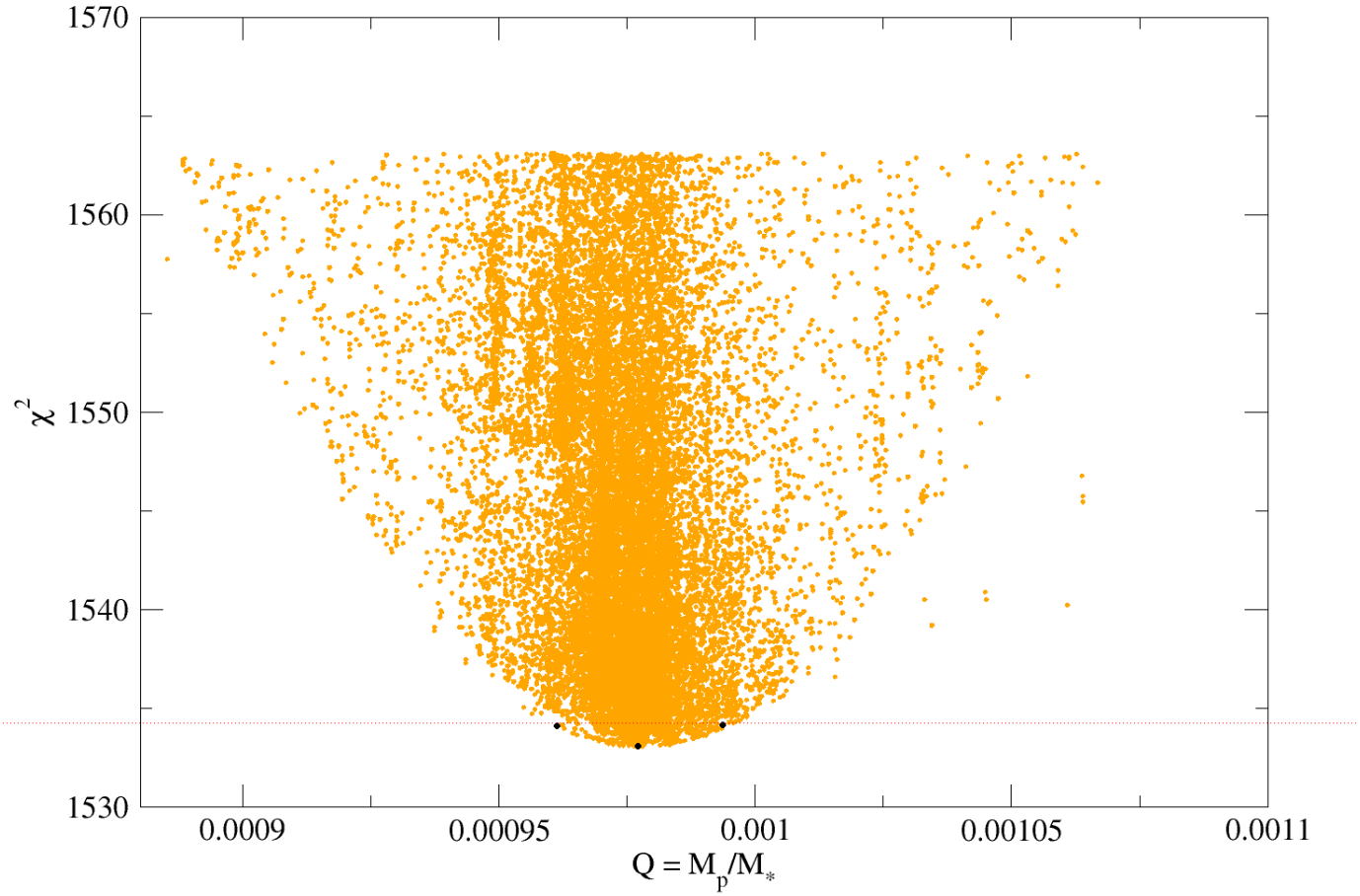

Fig. 15.— x^2 values resulting from geneticELC's guesses for M_*/M_p during its 1500-generation run. The values are mostly well-converged.

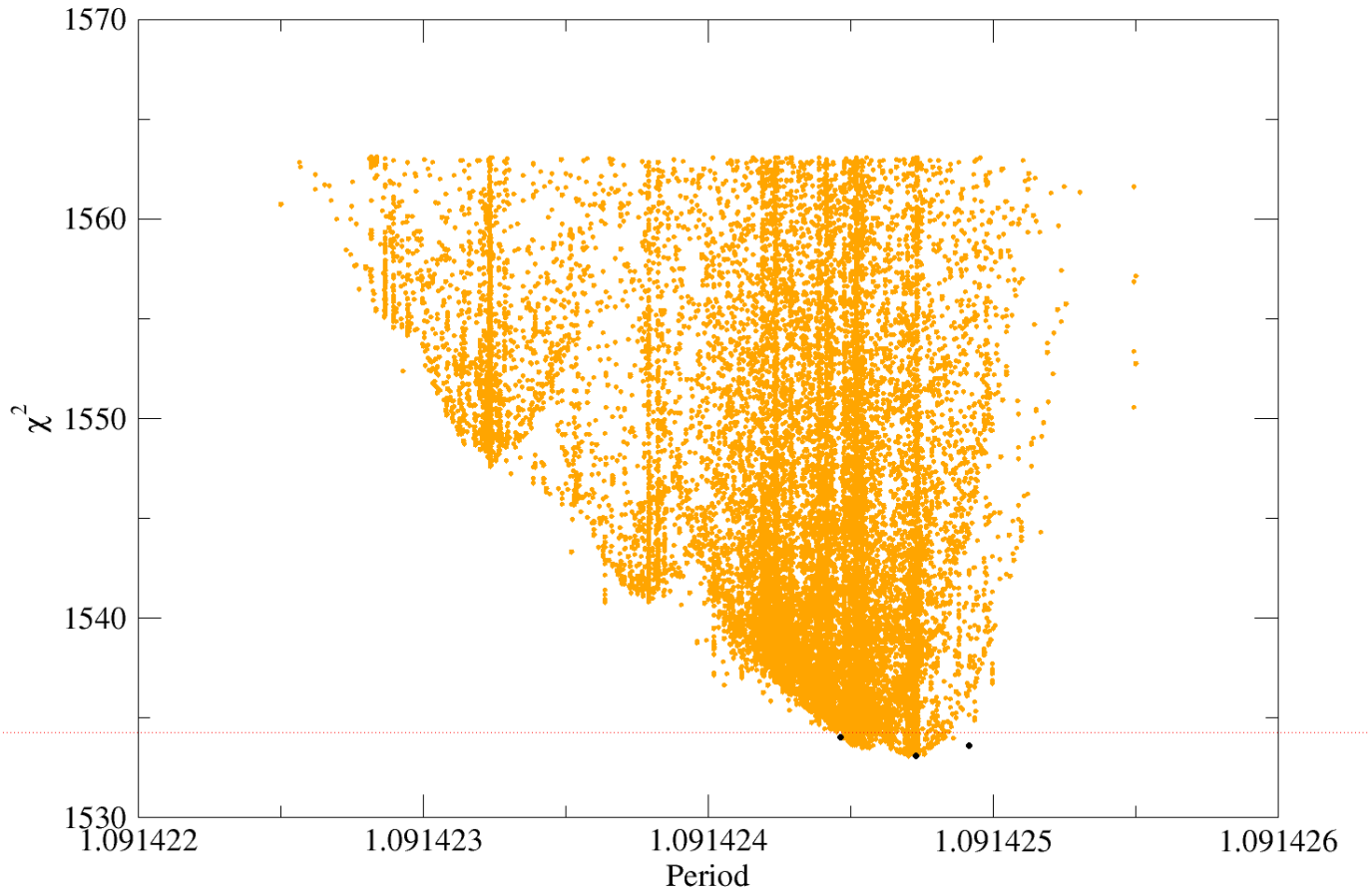

Fig. 16.— x^2 values resulting from geneticELC's guesses for *P* during its 1500-generation run. The values are well-converged.

Parameter	Our Value	Hebb et al. (2009)	Maciejewski et al. (2011)
i (deg)	$82.0143^{+0.3679}_{-0.0800}$	$83.1^{+1.4}_{-1.1}$	$82.5^{+0.8}_{-0.7}$
P (days)	$1.0914245^{+0.0000003}_{-0.0000002}$	$1.091423^{+0.000003}_{-0.000003}$	$1.09142245^{+0.00000033}_{-0.00000033}$
T_0 (BJD)	$2454508.425072^{+0.000175}_{-0.0001243}$	$2454508.9761^{+0.0002}_{-0.0002}$	$2454508.97682^{+0.00020}_{-0.00020}$
M_p/M ($\times 10^{-3}$)	$9.77200^{+0.01645}_{-0.01583}$	$9.97^{+0.13}_{-0.13}$ *	
M ($M_\odot$)	$1.29796^{+0.04417}_{-0.01513}$	$1.35^{+0.14}_{-0.14}$	
R/R_p	$8.45222^{+0.03218}_{-0.02000}$	$8.51^{+0.06}_{-0.06}$ *	$8.513^{+0.049}_{-0.049}$ *
R ($R_\odot$)	$1.62575^{+0.01447}_{-0.01040}$	$1.57^{+0.07}_{-0.07}$	$1.63^{+0.08}_{-0.08}$
K (km/s)	$0.21815^{+0.00366}_{-0.00356}$	$0.226^{+0.004}_{-0.004}$	
T_p/T	$0.20519^{+0.54541}_{-0.00519}$	$0.399^{+0.020}_{-0.009}$ *	$0.408^{+0.025}_{-0.012}$ *

Table 1: Best-fit parameters generated by geneticELC, and the corresponding best-fit values from Hebb et al. (2009) and Maciejewski et al. (2011). Blank spaces indicate that those values were not given in that publication (beyond references to previous publications), and asterisks (*) denote values we computed via related values in that publication. Errors on those parameters were propagated in quadrature from those given in those papers.

Parameter	Our Value
x_R	$0.149463^{+0.032343}_{-0.018708}$
y_R	$0.532248^{+0.048522}_{-0.103392}$
x_I	$1.000000^{+0.108000}_{-0.000000}$
y_I	$0.000000^{+0.015458}_{-0.000000}$

Table 2: Quadratic-law limb-darkening parameters for the R and I bands.

REFERENCES

Claret, A., & Bloeman, S. 2011, A&A, 529, A75

Eastman, J., Siverd, R., Gaudi, B. S. 2010, PASP, 122, 894

Hebb, L., Collier-Cameron, A., Loeillet, B., et al. 2009, ApJ, 693, 2

Maciejewski, G., Errmann, R., St. Raetz, Seeliger, M., Spaleniak, I., Neuhäuser, R. 2011, A&A, 528, A65

Orosz, J. A., & Hauschildt, P. H. 2000, A&A, 364, 265